Materials Science-Poland, 36(4), 2018, pp. 748-760
http://www.materialsscience.pwr.wroc.pl/
DOI: 10.2478/msp-2018-0099

Influence of magnetron powering mode on various properties of TiO_2 thin films

ARTUR WIATROWSKI[1], MICHAŁ MAZUR[1,*], AGATA OBSTARCZYK[1], DANUTA KACZMAREK[1], ROMAN PASTUSZEK[1], DAMIAN WOJCIESZAK[1], MARCIN GROBELNY[2], MAŁGORZATA KALISZ[2]

[1]Wroclaw University of Science and Technology, Faculty of Microsystem Electronics and Photonics, Janiszewskiego 11/17, 50-372 Wroclaw, Poland

[2]Motor Transport Institute, Centre for Material Testing, Jagiellonska 80, 03-301 Warsaw, Poland

In this paper, comparative studies on the structural, surface, optical, mechanical and corrosion properties of titanium dioxide (TiO_2) thin films deposited by continuous and sequential magnetron sputtering processes were presented. In case of continuous process, magnetron was continuously supplied with voltage for 90 min. In turn, in sequential process, the voltage was supplied for 1 s alternately with 1 s break, therefore, the total time of the process was extended to 180 min. The TiO_2 thin films were crack free, exhibited good adherence to the substrate and the surface morphology was homogeneous. Structural analysis showed that there were no major differences in the microstructure between coatings deposited in continuous and sequential processes. Both films exhibited nanocrystalline anatase structure with crystallite sizes of ca. 21 nm. Deposited coatings had high transparency in the visible wavelength range. Significant differences were observed in porosity (lower for sequential process), scratch resistance (better for sequential process), mechanical performance, i.e. hardness:elastic modulus ratio (higher for sequential process) and corrosion resistance (better for sequential process).

Keywords: *titanium alloys; TiO_2; sputtering; mechanical properties; structural properties; thin films*

1. Introduction

Several decades ago, the major application of titanium was in the aerospace industry, where mechanical properties were the primary consideration. In industrial applications, however, corrosion resistance is the most important property. Titanium, like any other metal, is a subject of corrosion in certain environments. The corrosion resistance of titanium is the result of a stable, protective, strongly adherent oxide film formed on its surface. The passive layer is built from a mixture of titanium oxides, mainly from TiO_2 (rutile) and Ti_2O_3 and TiO [1, 2] and provides titanium the resistance to corrosion as long as the integrity of the film is maintained. Typically, the thickness of passive films formed on these metals is about 3 nm to 10 nm [3]. The natural oxide is amorphous and stoichiometrically defective. It is known that the protective and stable oxides on titanium surfaces are able to provide favorable osseointegration. Such oxide films form instantly, when surface is exposed to air or moisture. The titanium oxide film is very stable, though relatively thin, and is affected only by few substances, most notable of which is hydrofluoric acid. Fluoride ions can dissolve the protective oxide film leading to obtaining a defective porous coating and losing its protectiveness, especially in acidic solutions [4]. One way to protect a titanium alloy surface from corrosion is application of coatings by surface modification techniques.

The main objectives of surface treatments mainly consist in the improvement of the tribological behavior, corrosion resistance and osseointegration of the metals. Coatings of enhanced wear and corrosion resistance can be manufactured by different surface modifications techniques, such as surface oxidation, physical deposition methods, like ion implantation and plasma spray coatings as well as thermo-chemical surface treatments, such as nitriding, carburizing and boriding [5, 6]. However,

*E-mail: michal.mazur@pwr.edu.pl

oxidation remains the most popular technique for the surface modification of titanium alloys. These oxide layers on titanium are commonly produced by either heat treatment [7–9] or electrolytic anodizing [10]. Thermal oxidation results in the formation of a 15 μm to 30 μm thick titanium dioxide layer of rutile phase. However, due to their long-term high temperature action, thermal diffusion processes can also lead to the formation of a diffusion sublayer consisting of an oxygen solid solution in α-Ti, and development of phase segregation and coalescence which may cause substrate embrittlement and worsened mechanical and/or corrosion performance. Titanium dioxide (TiO_2), which is also one of the most extensively studied metal oxides [11], finds wide, multifunctional application in e.g. photocatalysis, photochromic and electrochromic devices, biosensors, bactericide or optical devices [12–15] and for corrosion protection [11]. TiO_2 is characterized by high transparency over a visible wavelength range, wide band gap and high electrical resistivity at room temperature [16]. Moreover, it is a non-toxic material, which exhibits high mechanical, chemical and thermal stability. TiO_2 is one of "high-index" materials, which can be used in the construction of optical filters or antireflective coatings. It can be applied in various applications, such as protective coatings, self-cleaning coatings, gas sensing films, solar cells and antibacterial coatings [17–19]. Titanium dioxide thin films can be prepared by various deposition methods, e.g. evaporation, radio frequency (RF) or pulsed magnetron sputtering, laser or vacuum arc deposition [20–24]. Properties of thin oxide films strongly depend on their microstructure, roughness, porosity and crystallite sizes. Therefore, there is also a strong interest towards controlling these properties by suitable application of deposition process parameters.

In the present paper, the structural, surface, optical, mechanical and corrosion properties of titanium dioxide thin films deposited on, among others, Ti6Al4V titanium alloy by continuous and sequential magnetron sputtering processes were discussed.

2. Experimental

Titanium dioxide thin films were deposited using pulsed DC magnetron sputtering process. High purity (99.99 %) metallic Ti target was used as sputtering source. Magnetron with Ti target was powered by DPS pulsed DC power supply working in unipolar mode using 165 kHz sinusoidal pulses with the voltage amplitude of 1.8 kV. TiO_2 thin films were deposited in pure oxygen (without argon acting as a working gas) with a flow rate of 18 sccm (standard cubic centimeters per minute). Vacuum chamber was evacuated to a base pressure of ca. 5×10^{-3} Pa, while during sputtering, the pressure was equal to 2.4 Pa. Power supplied to the magnetron was equal to 550 W. Titanium dioxide coatings were prepared in two, slightly different processes, i.e. with constant and intermittent powering of the magnetron. In case of continuous powering, the magnetron was supplied with a constant voltage. In intermittent process, the magnetron was supplied with a voltage for 1 s and the supplying break was also equal to 1 s. Therefore, these processes were designated as continuous and sequential, respectively. The sputtering process times varied due to the change of powering conditions and were equal to 90 min for the continuous process and 180 min for the sequential one. The thickness of deposited thin films was measured with the aid of Taylor Hobson CCI Lite optical profiler and was equal to 560 nm and 580 nm for continuous and sequential processes, respectively.

Thin oxide films were deposited on silicon, fused silica and Ti6Al4V alloys. Microstructure and optical properties were measured using thin films deposited on fused silica, while surface morphology and cross-section were analyzed with the use of coatings sputtered on silicon. Moreover, thin films deposited on Ti6Al4V titanium alloys were employed for mechanical and electrochemical analysis. The surface of titanium alloys, before deposition, were polished on emery paper and diamond suspension up to 0.05 μm to a "mirror image".

Structural properties of as-deposited thin films were measured with the use of X-ray diffraction (XRD) employing PANalytical Empyrean

PIXcel^{3D} powder diffractometer with CuKα X-ray ($\lambda = 1.54056$ Å). The crystallite sizes were calculated using Scherrer equation [25] taking into consideration the broadening of apparatus and were verified with the use of MDI Jade software.

Raman spectra were measured using a Thermo Scientific DXR™ Raman Microscope instrument in the range of 70 cm^{-1} to 1000 cm^{-1} using 455 nm blue laser diode as an excitation source with a power of a light source equal to 6 mW. The exposure time of 10 s was applied and 25 scans were performed in each measurement.

Surface morphology and cross-section of deposited thin films were obtained using FESEM FEI Nova NanoSEM 230 scanning electron microscope (SEM) employing "through the lens detector" (TLD). Elemental composition of prepared coatings was investigated with the use of EDAX Genesis energy dispersive spectrometer (EDS). Measurements were performed in three different places for samples from each deposition process (continuous and sequential). The EDS used for measurements was calibrated for quantitative analysis and was accurate for qualitative analysis from approximately 0.1 at.%.

Transmission spectra were measured with the use of Ocean Optics QE65000 spectrophotometer and a coupled deuterium-halogen light source. Optical band gap energy E_g for direct transitions was determined on the basis of Tauc plots, while refractive indices and extinction coefficients were evaluated using reverse engineering method and FTG FilmStar software employing extended Cauchy model. Based on obtained values, porosity P and packing density PD of deposited thin films were analyzed.

The scratch resistance of the coatings was measured with the use of Taber Oscillating Abrasion Tester 6160. The oscillating sand tester is described in an ASTM F735 standard as a test method for determination of abrasion resistance. The primary application of the Oscillating Sand Abrasion Tester is for transparent materials and coatings utilized in windows and lenses, organic coatings, plastics, metals and other materials. The oscillating movement of the abrasive sand results in a random pattern of scratches that simulates everyday wear. The distance of sand tray stroke was equal to 100 mm at a speed of 300 strokes per minute and the abrasive medium was a 6/9 silica. Surface of transparent oxide thin films was examined for scratch resistance by optical microscope Olympus BX51 working in reflected light mode. Additionally, three-dimensional images of coating surface before and after scratch tests were obtained with the aid of TalySurf CCI Lite Taylor Hobson optical profiler.

The corrosion behavior of titanium alloy and alloy with thin films were examined using a three electrode cell setup by voltammetric measurements. The electrochemical cell consisted of silver/silver chloride reference electrode (Ag/AgCl) connected to the cell via a salt bridge with a luggin capillary, a platinum mesh as a counter electrode, and the working electrode (titanium alloy or titanium alloy with thin film). The exposed area of the sample surface limited by the cylinder inner wall was 0.236 cm^2. Voltammetric measurements were carried out with a scan rate of 1 mV/s within the range of –150 mV to 1000 mV versus open circuit potential (OCP) and polarization curves corresponding to every examined material were recorded. Prior to each polarization experiment, the samples were immersed in the electrolyte for 1 h, while monitoring the open circuit potential to establish steady state conditions. The measurements were carried out by means of Autolab EcoChemie System of AUTOLAB PGSTAT 302 N type equipped with GPESv. 4.9. software in aerated solutions at room temperature. The values of electrochemical parameters: i_{corr} – corrosion current density and E_{corr} – corrosion potential, were obtained from the voltammetric (polarization) curves by extrapolation of the cathodic and anodic branch of the polarization curves to the corrosion potential (Tafel extrapolation technique) [26]. All the electrochemical measurements were repeated at least three times to confirm the reproducibility of the results.

The hardness measurements of the thin films on Ti alloys were performed using

the nanoindenter manufactured by CSM Instruments (Switzerland) equipped with a diamond Vickers indenter. The hardness was calculated using the method proposed by Oliver et al. [27]. The measured hardness of the thin film deposited on a Ti6Al4V alloy can be expressed as a power-law function of the substrate and the thin film hardness, the depth of nanoindentation and the thickness of thin film [28]:

$$H = H_S\left(\frac{H_f}{H_S}\right)^M \tag{1}$$

where H_s is hardness of substrate, H_f is hardness of thin film, M is dimensionless spatial function defined by the following equation [28]:

$$M = \frac{1}{1+A\left(\frac{h}{d}\right)^B} \tag{2}$$

where A, B are adjustable coefficients, h is maximum intender displacement, d is the thickness of thin film.

Equation 1 must fulfil essential boundary conditions: when the indentation depth approaches zero (small indentation displacement), the measured hardness tends to the thin film hardness value, whereas, when the indentation depth approaches the thin film thickness, measured hardness tends to the value of substrate hardness.

3. Results

XRD patterns of as-deposited TiO_2 thin films are shown in Fig. 1a. The visible diffraction peaks are rather intense, indicating that the sputtered coatings are well crystallized. Both thin films exhibit nanocrystalline anatase structure. The average crystallite sizes, calculated using Debye-Scherrer formula [25] from the full width at half maximum (FWHM), and confirmed with the use of Jade software, were equal to ca. 21.0 nm to 21.5 nm for (1 0 1) plane for both deposited thin films. Taking into consideration high signal-to-noise ratio, the determination of crystallites dimensions could be encumbered with a slight error. XRD analysis showed that there are no major differences in microstructure between coatings deposited in continuous and sequential processes. Additionally, the broadening of the peak intensities of XRD pattern at 20° to 25° (2θ) is related to the amorphous fused silica substrate on which both TiO_2 thin films were deposited. A small shift towards lower angle (2θ) of the (1 0 1) peak, visible in the XRD patterns, indicates the possible presence of a tensile stress of ca. 0.2 %. The type of the stress occurring in crystal structure was determined based on Δd parameter, which is the relative difference in the interplanar distances between measured (d) and standard ones (d_{PDF}) [29–31]:

$$\Delta d = \frac{d - d_{PDF}}{d_{PDF}} \cdot 100\% \tag{3}$$

where d is interplanar distance in the thin film, d_{PDF} is the standard interplanar distance from PDF Card [32].

Additionally, the comparison of the unit cell parameters and volume of as-deposited TiO_2 thin films is shown in Table 1. For determination of the unit cell parameters of the tetragonal crystal structure, following equation was used:

$$\frac{1}{d^2} = \frac{h^2+k^2}{a^2} + \frac{l^2}{c^2} \tag{4}$$

where d is interplanar distance in the thin film; a, c are the unit cell lattice parameters; h, k, l are Miller indices of a crystal plane.

The unit cell parameters of both deposited thin films are slightly higher than those of the bulk cell reported in the literature [32]. The volume of TiO_2 cell deposited in continuous process is larger than that obtained from the sequential one, which might also confirm the results reported for calculated tensile stress. Summary of XRD results is shown in Table 1.

Microstructure of prepared coatings was also analyzed and supplemented with the use of Raman spectroscopy, which showed all expected vibrational modes of TiO_2-anatase (Fig. 1b). Anatase phase is tetragonal and has six Raman active modes that occur at ca. 144 cm^{-1} E_g, 197 cm^{-1} E_g, 398 cm^{-1} B_{1g}, 515 cm^{-1} A_{1g}, 519 cm^{-1} B_{1g} and 640 cm^{-1} $3E_g$ [33]. Raman spectra presented

Table 1. XRD measurements results and comparison of the unit cell parameters and primitive cell volume of TiO_2 thin films deposited in various magnetron sputtering processes.

Thin film	MS process	Phase	D [nm]	d [nm]	Δd [%]	Type of stress	a [Å]	c [Å]	V [Å^3]
TiO_2	PDF #21-1272	anatase	–	d_{PDF} 0.3520	–	–	3.7852	9.5139	136.31
	sequential		21.5	0.3526	+0.17	tensile	3.7900	9.6157	138.12
	continuous		21.0	0.3528	+0.22	tensile	3.7866	9.7066	139.21

Designations: D is an average crystallites size, d is interplanar distance; d_{PDF} is a standard interplanar distance; Δd is a relative difference in interplanar distances between measured d and standard ones d_{PDF}; $\Delta d = [(d - d_{PDF})/d_{PDF}] \times 100$ %; a, c are the unit-cell lattice parameters (length of the cell edges); V is the unit cell volume.

in Fig. 1b are in good agreement with reference values and shift of only few wave numbers equal to instrumental error bar. Characteristic Raman peaks which are observed at ca. 396 cm^{-1}, 517 cm^{-1} and 638 cm^{-1} suggest that the microstructure of deposited coatings consists of high purity anatase phase, while the intensity and sharpness of these peaks testifies the occurrence of highly crystalline structure. It is worth noting that peaks related to rutile phase are not observed. Additionally, there is no major difference between Raman spectra of thin films sputtered in continuous and sequential processes. These results are in good agreement with the X-ray diffraction studies.

Based on SEM images (Fig. 2) it can be seen that there is a major difference in the morphology of TiO_2 thin films. The surface of each coating is densely packed and crack free. Both coatings have a columnar structure, which can be directly observed at the cross-section images. Additionally, the growth of the columns perpendicular to the substrate has been marked with red lines for both coatings. In case of the film deposited in sequential process, significantly larger column diameters can be observed as-compared to the coating prepared with continuous powering of the magnetron. The average size of the columns at the top is about 200 nm to approximately 300 nm for TiO_2 deposited in sequential process, while for continuous process it is only ca. 100 nm. Moreover, the microstructure of the film from sequential sputtering also consists of a great number of smaller columns with a diameter of ca. 30 nm to approximately 60 nm. Additionally, at the beginning of the thin film growth in the continuous process it seems that the growth was not columnar. However, after some time of sputtering, the columns began to arise and their thickening with a film growth was also observed. This may testify the presence of some volume of amorphous phase in the film deposited by the continuous process.

Obtained spectra of EDS measurements for both thin films are presented in Fig. 2c and show peaks related only to titanium, oxygen and silicon. Signal from SiKα line has been obtained from the silicon substrate used during the measurement, while titanium and oxygen are related to the deposited thin films. Such spectra show high purity of prepared coatings and lack of impurities, which could have an impact on the thin film growth and formation of its microstructure. This means that the structural properties of both coatings are directly dependent on the conditions of each sputtering process. Furthermore, due to application of pure oxygen during deposition (without argon acting as a working gas) it can be assumed that all coatings were fully oxidized. Previous experiences with thin films deposited in such processes proved that obtained coatings were stoichiometric [34]. Additionally, taking into consideration that all thin films are well transparent and XRD and Raman spectroscopy studies revealed only TiO_2-anatase phase, it can be stated that the deposited coatings are free of TiO_x-related crystal phases.

Transmission spectra of deposited thin films are presented in Fig. 3a. Both thin films are well transparent in the visible wavelength range with average transparency of ca. 80 %. Visible maxima

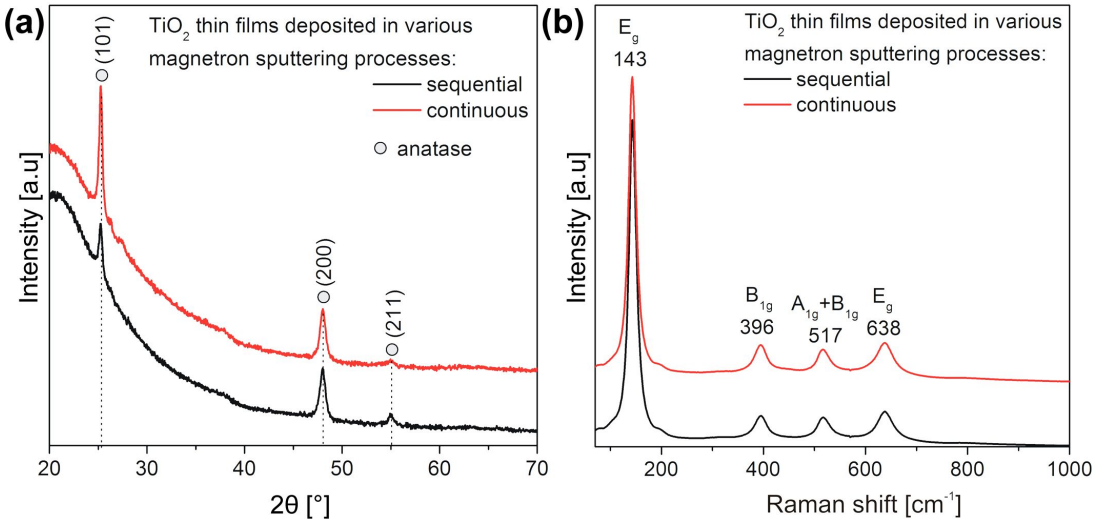

Fig. 1. Microstructure investigation results: (a) XRD patterns and (b) Raman spectra.

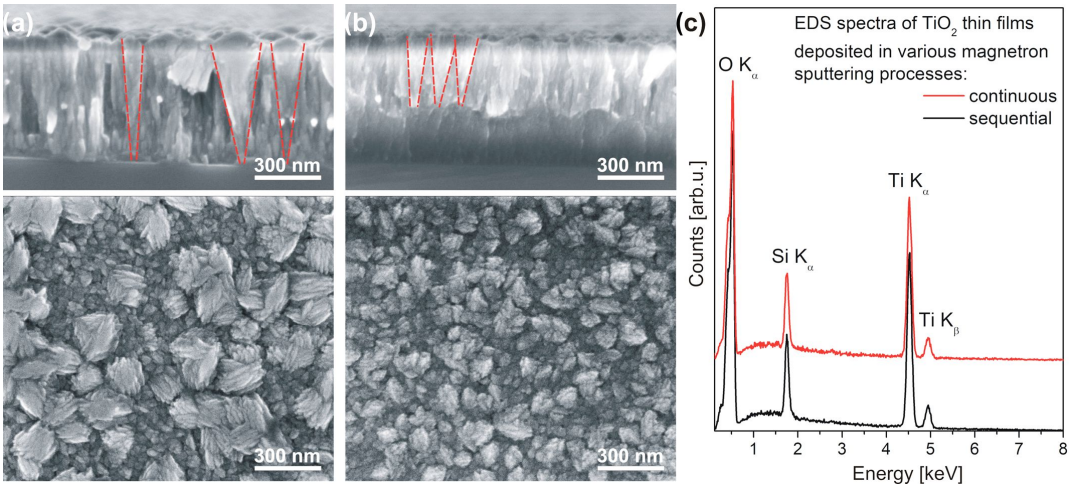

Fig. 2. SEM images of cross-section and surface of TiO_2 thin films deposited in various magnetron sputtering processes: (a) sequential, (b) continuous and (c) EDS spectra of both samples.

and minima, i.e. interference effects, are the result of light reflection from the thin films and thin film-substrate interface. Analysis of the cut-off wavelength showed that its value was very similar for both coatings and equal to 345 nm and 347 nm for samples deposited in sequential and continuous processes, respectively. Optical band gap energy (Fig. 3b) was calculated with the use of Tauc plots $(\alpha h\nu)^{1/2}$ in the function of photon energy (eV) [35]:

$$\alpha h\nu = \alpha_1 \left(h\nu - E_g{}^{opt}\right)^2 \tag{5}$$

where: h is Planck constant, ν is radiation frequency, α_1 is constant coefficient.

Larger value of E_g was obtained for thin film deposited in sequential process, however, similarly to $\lambda_{cut-off}$ the difference was negligible.

Observation of the transmission spectra amplitude revealed that it was slightly larger for thin films deposited in sequential process, which might testify the higher value of refractive index n. The real and imaginary parts of the refractive index were calculated using reverse engineering method applying generalized Cauchy model. As it was

assumed, with the use of FTG FilmStar software, the higher value of refractive index was obtained for thin film deposited by magnetron sputtering with sequential powering. Additionally, analysis of extinction coefficient k showed that the lower value was exhibited by TiO_2 thin film from sequential process, which is favorable due to the lower optical losses of this coating. Spectra of refractive index and extinction coefficient of deposited coatings are presented in Fig. 3c and Fig. 3d, respectively.

Due to possible application of deposited thin films in optoelectronic or optical devices or as protective coatings it is crucial to evaluate their tribological properties. The scratch resistance of the coatings was evaluated based on the oscillating sand test. The evaluation of thin films surface before (Fig. 4, left side) and after performing scratch tests (Fig. 4, right side) was performed with the use of optical profiler (3D images) and microscope. Additionally, the root mean square Sq roughness and surface profiles were analyzed. Results of performed measurements revealed that both coatings before scratch tests had homogenous and smooth surfaces with low root mean square RMS roughness of 1.11 nm (continuous process) and 1.36 nm (sequential process). After performing oscillating sand tests the roughness of the coatings increased to 2.01 nm and 1.60 nm for continuous and sequential processes, respectively. Based on optical profiler and microscope images the surface of thin films after abrasion tests did not reveal major scratches and only negligible changes could be observed. Additionally, the surface profile amplitude (shown as charts) did not increase greatly. Taking into consideration the obtained results it can be assumed that slightly better scratch resistance was observed for thin films sputtered with sequentially powered magnetron.

Nanoindentation results showed that both TiO_2 coatings have very similar hardness ranging from ca. 10 GPa to 10.1 GPa. In turn, there is a difference in the Young elastic modulus, which is much lower for the thin films from sequential process. The difference is equal to ca. 20 %. The results of mechanical tests are shown in Fig. 5. Results of mechanical and tribological analysis are summarized in Table 2.

Electrochemical measurements of deposited thin films are presented in Fig. 6. The calculated corrosion current density i_{corr} for TiO_2 on titanium alloy were found 8.13×10^{-6} A·cm^{-2} and 2.72×10^{-7} A·cm^{-2} for continuous and sequential magnetron sputtering process, respectively. The above results show that a low electrochemical activity, confirmed by low corrosion currents densities, was achieved for TiO_2 films deposited on the titanium alloy surface. However, the smallest corrosion current density and therefore the best corrosion properties, were obtained for TiO_2 thin film deposited in sequential magnetron sputtering processes. Electrochemical parameters for as-received Ti6Al4V titanium alloy, obtained under the same measuring conditions, were: $i_{corr} = 7.28 \times 10^{-4}$ A·cm^{-2} and $E_{corr} = -0.931$ V.

Furthermore, TiO_2 deposited in sequential magnetron sputtering process, is characterized by a stable course of open cell potential OCP (Fig. 6a). In case of the oxide coating deposited in continuous magnetron sputtering process, gradual change in the OCP value in a more negative direction occurs. This may be due to the gradual dissolution of the oxide layer, as is the case of titanium without the coating.

Table 2. Results of mechanical and electrochemical measurements of TiO_2 thin films deposited on Ti6Al4V alloy by various magnetron sputtering processes.

	Magnetron sputtering process	
	Continuous	Sequential
Hardness [GPa]	10.1	10.0
Young elastic modulus [GPa]	169.4	137.1
H^3:E^2	0.036	0.053
RMS – before scratch test [nm]	1.11	1.36
RMS – after scratch test [nm]	2.01	1.60
i_{corr} [A·cm^{-2}]	8.13×10^{-6}	2.72×10^{-7}
E_{corr} [V]	–0.801	0.116

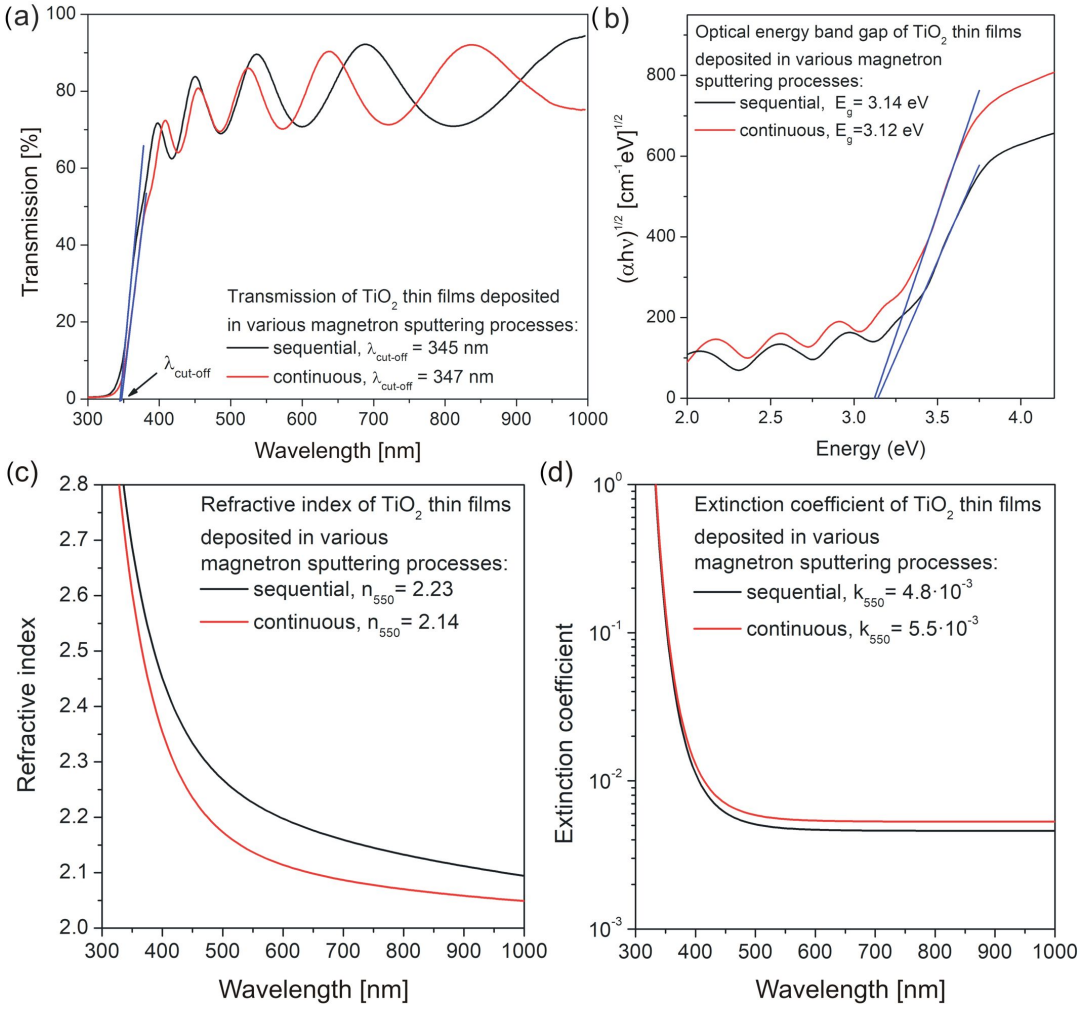

Fig. 3. Comparison of optical properties of TiO_2 thin films deposited in continuous and sequential processes: (a) transmission spectra with determined $\lambda_{cut-off}$, (b) optical band gap, (c) refractive index and (d) extinction coefficient.

4. Discussion

The results presented in this paper showed that the modification of magnetron powering parameters led to deposition of TiO_2 coatings with various properties. It should be noted that, though a well-crystallized anatase structure was obtained in both cases, the subtle differences in the crystallization process on the substrate during the deposition had an effect on the optical, mechanical and electrochemical properties of the nanocrystalline TiO_2 films. It is well known that pulsed DC and RF discharges prevent electric instabilities due to arcing occurring when insulating compounds, such as TiO_2, are deposited with the use of reactive magnetron sputtering. Additionally, in the literature there are few reports regarding so-called low-frequency modulation of magnetron sputtering [36–38] in which, for example, a controlled poisoning of the target by the reactive gas (oxygen) and its cleaning by the sputtering are alternately realized, which is favorable in case of manufacturing titania coatings. Such a phenomenon leads to stable conditions of sputtering allowing simultaneously to the formation of stoichiometric thin films on the substrate. In case of the presented titanium dioxide films, both processes were performed using pulsed DC power supply working in unipolar mode

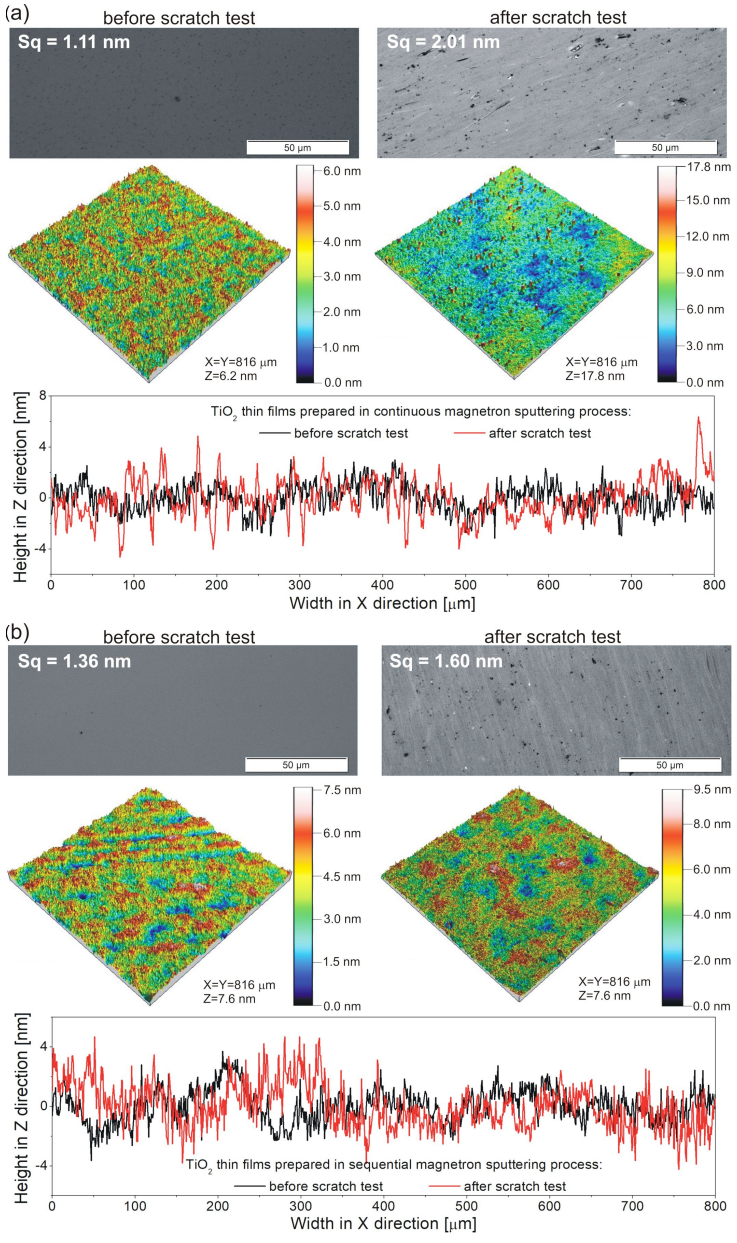

Fig. 4. Results of surface geometry measurements for TiO_2 thin films deposited in: (a) continuous and (b) sequential magnetron sputtering processes before and after scratch tests.

using 165 kHz sinusoidal pulses with the maximum voltage amplitude of 1.8 kV. All sputtering conditions, such as pressure during the deposition, power delivered to the magnetron with titanium metallic target and the target-substrate distance, were kept the same for continuous and sequential processes. The only change incorporated to the sequential process was supplying the magnetron in a low frequency manner, i.e. magnetron was supplied with voltage for 1 s and supplying break was also equal to 1 s. The authors believe that variations of the plasma flux distribution had a substantial influence on the mechanism of thin films crystallization, growth and surface activation that were responsible for further changes of TiO_2 properties. Up to date there are only few materials,

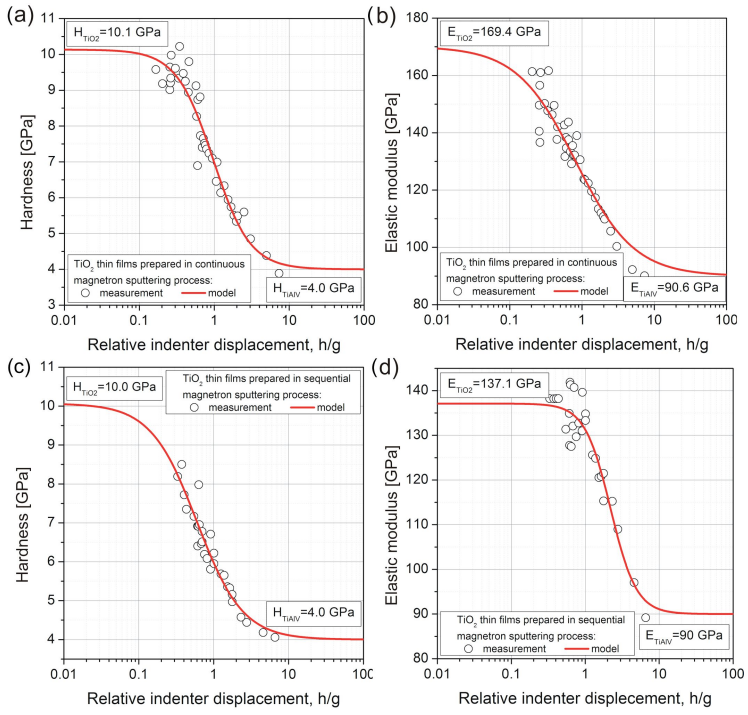

Fig. 5. Results of hardness (left side) and Young elastic modulus (right side) of TiO_2 thin films deposited by: (a), (b) continuous and (c), (d) sequential magnetron sputtering processes.

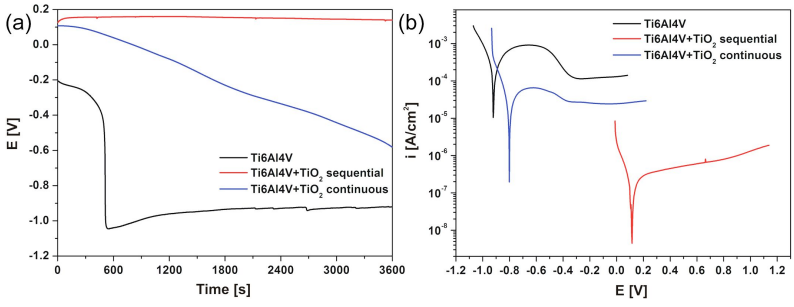

Fig. 6. Open circuit potentials and voltammetric curves of Ti6Al4V and titanium alloy with TiO_2 thin films deposited by various magnetron sputtering processes.

such as ITO, Al_2O_3 or MoN_x, that have been prepared using low-frequency magnetron sputtering [36–38]. However, there is a lack of reports about the properties of such titanium dioxide coatings. Therefore, in this paper TiO_2 thin films were prepared with the use of continuous and sequential magnetron sputtering processes and their structural, optical, mechanical and electrochemical properties were compared.

In case of microstructure analysis only slight changes between both films were observed. Nevertheless, performed studies of optical properties regarding packing density and porosity showed the differences between deposited coatings which could also directly influence their mechanical properties. The refractive index of thin films is dependent on their density which could be explained by the well-known Clausius-Mossotti relation [39, 40]. The packing density PD can be defined as the density ratio of the film and the bulk material. Taking into consideration determined values of refractive index of deposited thin films (at the wavelength of 550 nm) it was possible

to calculate their packing density and porosity [41–44]. Lower porosity and simultaneously higher packing density were obtained for thin film deposited by sequential powering of magnetron. Porosities of TiO_2 coatings from continuous and sequential processes were equal to ca. 31.0 % and 23.5 %, respectively. In turn, the packing density was equal to 0.86 and 0.90 for thin film from continuous and sequential processes, respectively.

Deposition parameters also influenced the mechanical properties of TiO_2 thin films. It is well known that the resistance against elastic strain to failure can be evaluated based on H^3:E^2 ratio and it is considered as an important parameter in case of investigating tribological performance of prepared coatings. The H^3:E^2 value provides information about the resistance of materials to plastic deformation [45, 46]. This ratio shows that the plastic deformation of a coating can be reduced when it exhibits both a high hardness and a low elastic modulus. H^3:E^2 ratio can be influenced by the structural properties (e.g. crystallite sizes), microstructure stresses or amount of amorphous phase occurring in the thin film [47–49]. In case of both coatings the hardness was almost the same, however higher Young elastic modulus was obtained for the coating prepared by continuous process. Therefore, larger value of hardness:elastic modulus ratio and simultaneously better mechanical performance was obtained for TiO_2 thin film deposited with the use of sequential magnetron sputtering process.

Taking into account the results of structural studies as well as microscopic observations of prepared TiO_2 coatings, it can be concluded that the presence of amorphous areas between the columns improved tribological and mechanical properties of the coatings. Both films were composed of crystallites with an average size of about 21 nm (Table 2) that formed elongated columns. As a result, nanocrystalline anatase coatings with the same hardness of 10 GPa were obtained. However, in case of TiO_2 from sequential process, the presence of amorphous areas between columns allowed one to obtain lower value of Young modulus. Such a change was advantageous due to lower susceptibility to scratching and brittle cracking of the coating. Moreover, in case of thin film deposited in the sequential process the possible presence of amorphous phase at the boundaries of crystallites and elongated columns can lead to the stress relaxation caused by the dislocations. Therefore, the deformation of the elongated columnar crystallites during nanoindentation measurements does not generate simultaneous deformation of adjacent columns leading, as a result, to increased hardness. It should be also emphasized that the hardness of both coatings was very high and was equal to 10 GPa. TiO_2 coatings with anatase structure in majority of works presented in the literature [50–54] have hardness in the range of 3 GPa to 9 GPa. Wide range of this parameter is related to the fact that mechanical properties strongly depend not only on a material type, but also manufacturing method, microstructure, crystallite size and density of the material. That is why modification of the deposition process parameters can lead to the change of various properties of TiO_2. Moreover, even the post-process annealing at high temperature, accompanied by a phase transformation from anatase to rutile, does not guarantee hardness greater than 10 GPa. Therefore, such a high hardness of TiO_2 thin films with anatase structure, prepared in a sequential process, combined with their relatively small value of Young modulus gives great application potential. Due to the anatase microstructure of the deposited thin films they could be used as transparent photocatalytic coatings in window panes for automotive or building industry. On the other hand, very good mechanical properties and scratch resistance promote application of such coatings in ophthalmics as a material for glass lenses. It is also worth noting that very good mechanical properties combined with a high corrosion resistance, give a possibility of application of those coatings in medicine, e.g. as protective films for various types of implants.

5. Conclusions

The investigation of structural, surface, optical, mechanical and corrosion properties of titanium dioxide thin films deposited on Ti6Al4V titanium

alloy by continuous and sequential magnetron sputtering processes, led to the following conclusions:

- XRD and Raman analysis showed that there were no major differences in microstructure between the coatings deposited in continuous and sequential processes. Both titanium dioxide thin films exhibited nanocrystalline structure of high purity anatase.
- Both thin films were well transparent in the visible wavelength range with average transparency of ca. 80 %.
- Lower porosity (23.5 %) and simultaneously higher packing density was obtained for thin film deposited by magnetron sputtering process with sequential powering, exhibiting larger value of refractive index. In case of coatings from continuous process, porosity was equal to ca. 31 %. The packing density was equal to 0.86 and 0.90 for thin film prepared by continuous and sequential processes, respectively.
- Better scratch resistance was obtained for thin films sputtered using sequential powering of the magnetron.
- The hardness was almost the same, however higher Young elastic modulus was measured for the coating prepared by continuous process. Larger value of hardness: elastic modulus ratio and simultaneously better mechanical performance was obtained for TiO_2 thin film deposited with the use of sequential magnetron sputtering process.
- Titanium dioxide thin film deposited in sequential and continuous magnetron sputtering processes increased the corrosion resistance of the Ti6Al4V titanium alloy, but more effective protection, i.e. smallest corrosion current density, provided TiO_2 deposited in sequential process.

Acknowledgements

This work was co-financed from the sources given by the Ministry of Science and Higher Education within the Iuventus Plus Program (No. IP2014 029473) in the years of 2015 to 2017, from the Statutory Sources Number 0401/0130/18 and as a Research Project for Young Scientists Number 0402/0046/17.

References

[1] Bordji K., Jouzeau J.Y., Mainard D., Payan E., Netter P., Rie K.T., Stucky T., Hage-Ali M., *Biomaterials*, 17 (1996), 929.
[2] Zhu X., Chen J., Scheideler L., Reichl R., Geis-Gesrstorfer J., *Biomaterials*, 25 (2004), 4187.
[3] Neoh K.G., Hu X., Zheng D., Tang Kang E., *Biomaterials*, 33 (2012), 2813.
[4] Wang Z.B., Hu H.X., Liu C.B., Zheng Y.G., *Electrochim. Acta*, 135 (2014), 526.
[5] Carapeto A.P., Serro A.P., Nunes B.M.F., Martins M.C.L., Todorovic S., Duarte M.T., André V., Colaço R., Saramago B., *Surf. Coat. Tech.*, 204 (2010), 3451.
[6] Ma G., Gong S., Lin G., Zhang L., Sun G. A., *Appl. Surf. Sci.*, 258 (2012), 3045.
[7] Han Y., Hong S.H., Xu K.W., *Surf. Coat. Tech.*, 154 (2002), 314.
[8] Huang P., Wang F., Xu K., Han Y., *Surf. Coat. Tech.*, 201 (2007), 5168.
[9] Lange R., Lüthen F., Beck U., Rychly J., Baumann A., Nebe B., *Biomol. Eng.*, 19 (2002), 255.
[10] Huang P., Xu K-W., Han Y., *Mater. Lett.*, 59 (2005), 185.
[11] Kalisz M., Grobelny M., Świniarski M., Mazur M., Wojcieszak D., Zdrojek M., Judek J., Domaradzki J., Kaczmarek D., *Surf. Coat. Tech.*, 290 (2016), 124.
[12] Toma F-L., Bertrand G., Chwa S.O., Meunier C., Klein D., Coddet C., *Surf. Coat. Tech.*, 200 (2006), 5855.
[13] Daoud W.A., Xin J.H., *J. Sol-Gel Sci. Techn.*, 29 (2004), 25.
[14] Yoldas B.E., *Appl. Opt.*, 19 (1980), 1425.
[15] Nasimento G.L.T., Seara L.M., Neves B.R.A., Mohallem N.D.S., *Prog. Coll. Pol. Sci.*, 128 (2004), 227.
[16] Wojcieszak D., Mazur M., Indyka J., Jurkowska A., Kalisz M., Domanowski P., Kaczmarek D., Domaradzki J., *Mater. Sci-Poland*, 33 (3) (2015), 660.
[17] Domaradzki J., Kaczmarek D., Prociow E.L., Borkowska A., Kudrawiec R., Misiewicz J., Schmeisser D., Beuckert G., *Surf. Coat. Tech.*, 200 (2006), 6283.
[18] Twu M.J., Chiou A.H., Hu C.C., Hsu C.Y., Kuo C.G., *Polym. Degrad. Stabil.*, 117 (2015), 1.
[19] Choi K.H., Duraisamy N., Muhammad N.M., Kim I., Choi H., Jo J., *Appl. Phys. A*, 107 (2012), 715.
[20] Mazur M., Wojcieszak D., Kaczmarek D., Domaradzki J., Zatryb G., Misiewicz J., Morgiel J., *Opt. Mater.*, 42 (2015), 423.
[21] Jouanny I., Labdi S., Aubert P., Buscema C., Maciejak O., Berger M.H., Guipont V., Jeandin M., *Thin Solid Films*, 518 (2010), 3212.
[22] Zywitzki O., Modes T., Sahm H., Frach P., Goedicke K., Glos D., *Surf. Coat. Tech.*, 180 – 181 (2004), 538.

[23] BENDAVID A., MARTIN P.J., TAKIKAWA H., *Thin Solid Films*, 360 (2000), 241.
[24] SUDA Y., KAWASAKI H., UEDA T., OHSHIMA T., *Thin Solid Films*, 453 – 454 (2004), 162.
[25] KLUG H.P., ALEXANDER E.E., *X-ray diffraction procedures for polycrystalline and amorphous materials*, 2nd ed., John Wiley and Sons, New York, 1974.
[26] MANSFELD F., *Electrochemical Methods of Corrosion Testing*, in CRAMER S.D., COVINO B.S. JR. (Eds.), *Corrosion: Fundamentals, Testing, and Protection*, Vol. 13A. ASM Handbook, ASM International, 2003, pp. 446 – 462.
[27] OLIVER W.C., PHARR G.M., *J. Mater. Res.*, 7 (1992), 1564.
[28] JUNG Y.-G., LAWN B.R., MARTYNIUK M., HUANG H., HU X.Z., *J. Mater. Res.*, 19 (2004), 3076.
[29] DOMARADZKI J., KACZMAREK D., PROCIOW E., WOJCIESZAK D., SIERADZKA K., MAZUR M., *Opt. Appl.*, 39 (4) (2009), 815.
[30] WOJCIESZAK D., MAZUR M., KACZMAREK D., MORGIEL J., ZATRYB G., DOMARADZKI J., MISIEWICZ J., *Opt. Mater.*, 48 (2015), 172.
[31] MAZUR M., WOJCIESZAK D., DOMARADZKI J., KACZMAREK D., PONIEDZIAŁEK A., DOMANOWSKI P., *Mater. Res. Bull.*, 72 (2015), 116.
[32] *Powder Diffraction File*, Joint Committee on Powder Diffraction Standards, ASTM, Philadelphia, PA, Card 21-1272 – PDF.
[33] ALHOMOUDI I.A., NEWAZ G., *Thin Solid Films*, 517 (2009), 4372.
[34] MAZUR M., *Opt. Mater.*, 69 (2017), 96.
[35] TAUC J., *Optical Properties of Solids*, Amsterdam, North Holland, 1970.
[36] WICHER B., CHODUN R., NOWAKOWSKA-LANGIER K., OKRASA S., TRZCIŃSKI M., KRÓL K., MINIKAYEV R., SKOWROŃSKI Ł., KURPASKA Ł., ZDUNEK K., *Appl. Surf. Sci.*, 456 (2018), 789.
[37] BILLARD A., FRANTZ C., *Surf. Coat. Tech.*, 86 – 87 (1996), 722.
[38] JUNG S.K., LEE S.H., LEE Y.S., LEE S.M., PARK L.S., SOHN S.H., *Mol. Cryst. Liq. Cryst.*, 499 (2009), 316.
[39] KITTEL C., *Solid State Physics*, John Wiley & Sons, New York, 1971.
[40] HEITMANN W., *Thin Solid Films*, 5 (1970), 61.
[41] KERMADI S., AGOUDJIL N., SALI S., ZOUGAR L., BOUMAOUR M., BROCH L., NACIRI A., PLACIDO F., *Spectrochim. Acta A*, 145 (2015), 145.
[42] SUBRAMANIAN M., VIJAYALAKSHMI S., VENKATARAJ S., JAYAVEL R., *Thin Solid Films*, 516 (2008), 3776.
[43] DAVE V., DUBEY P., GUPTA H.O., CHANDRA R., *Thin Solid Films*, 549 (2013), 2.
[44] BAUER G., *Ann. Phys.-Berlin*, 411 (4) (1934), 434.
[45] MAZUR M., HOWIND T., GIBSON D., KACZMAREK D., SONG S., WOJCIESZAK D., ZHU W., MAZUR P., DOMARADZKI J., PLACIDO F., *Mater. Design*, 85 (2015), 377.
[46] CHANG L.C., CHANG C.Y., CHEN Y.I., *Surf. Coat. Tech.*, 280 (2015), 27.
[47] TSUI T.Y., PHARR G.M., OLIVER W.C., BHATIA C.S., WHITE R.L., ANDERS S., ANDERS A., BROWN I.G., *Mat. Res. Soc. Symp. Proc.*, 383 (1995), 447.
[48] Sergueeva A.V., Stolyarov V.V., Valiev R.Z., Mukherjee A.K., *Scripta Mater.*, 45 (2001), 747.
[49] WANG Y.M., OTT R.T., BUUREN T.V., WILLEY T.M., BIENER M.M., HAMZA A.V., *Phys. Rev. B*, 85 (2012), 014101.
[50] LIN J., WANG B., SPROUL W.D., OU Y., DAHAN I., *J. Phys. D Appl. Phys.*, 46 (2013), 084008.
[51] CHUANG L.C., LUO C.H., YANG S., *Appl. Surf. Sci.*, 258 (2011), 297.
[52] DUYAR O., PLACIDO F., DURUSOY H.Z., *J. Phys. D Appl. Phys.*, 41 (2008), 095307.
[53] SCHMIDT-STEIN F., THIEMANN S., BERGER S., HAHN R., SCHMUKI P., *Acta Mater.*, 58 (2010), 6317.
[54] MAYO M.J., SIEGEL R.W., NARAYANASAMY A., NIX W.D., *J. Mater. Res.*, 5 (5) (1990), 1073.

Received 2018-11-08
Accepted 2018-11-24